

Novel flexible bifunctional amperometric biosensor based on laser engraved porous graphene array electrodes: Highly sensitive electrochemical determination of hydrogen peroxide and glucose

Zhiwei Lu^{a,*}, Lan Wu^b, Xianxiang Dai^a, Yanying Wang^a, Mengmeng Sun^a, Cailong Zhou^c, Haijun Du^{d,*}, Hanbing Rao^{a,*}

^a College of Science, Sichuan Agricultural University, Xin Kang Road, Yucheng District, Ya'an 625014, PR China

^b School of Chemistry and Chemical Engineering, South China University of Technology, Guangzhou 510641, PR China

^c School of Chemistry and Chemical Engineering, Chongqing University, Chongqing 400044, PR China

^d School of Chemical Engineering, Guizhou Minzu University, Guiyang 550025, PR China

ARTICLE INFO

Editor: C. LingXin

Keywords:

Laser-engraved porous graphene (LEPG)

Electrochemical deposition

Flexible sensor

Glucose oxidases (GOD)

Pt nanoparticles (Pt NPs)

ABSTRACT

Polyimide-laser-engraved porous graphene (LEPG) are hopeful electrode modification materials for flexible electrochemical sensing based on its high-efficiency preparation and low cost. Herein, a flexible, multi-patterned, and miniaturized electrode was fabricated via a simple and novel direct laser engraving. 3D LEPG with porous network structure can selectively decorated with Pt nanoparticles (Pt NPs) by *in situ* electrochemical depositions (Pt-LEPG) as sensitively H₂O₂ sensors with a wide range of linear (0.01–29 nM) and high sensitivity (575.75 μA mM⁻¹ cm⁻²). Subsequently, a glucose biosensor was successfully constructed through immobilized glucose oxidases (GOD) onto Pt-LEPG electrode. New-designed GOD/Pt-LEPG glucose sensor exhibited a noteworthy lower limit of detection (0.3 μM, S/N = 3) and high sensitivity (241.82 μA mM⁻¹ cm⁻²), as much a wide-range of linear (0.01–31.5 mM) at near-neutral pH conditions, enabling detect glucose in real human serum specimens with satisfactory results. Predictably, these outstanding performance sensors have great potential in terms of flexible and wearable electronics.

1. Introduction

Hydrogen peroxide (H₂O₂) belongs to hazardous chemicals and chemical threat agent, is also one of the carcinogens published by the World Health Organization (WHO), formerly as a bleaching agent, fungicide, preservative widely used in food (Su et al., 2020; Zhang et al., 2009). However, the transportation and storage of high concentrations of H₂O₂ are of great risks, presenting a major limitation for its application. It is toxic due to its deleterious effects the central nervous system, disturbing DNA genetic molecule synthesis as well as causing neuro-psychiatric disorders (Kim et al., 2020). In biological systems, H₂O₂ belongs to the reactive oxygen species (ROS) group, compounds naturally found in our body tissues that are essential for normal cell functions and are inevitably generated. However, the inherent formation of ROS is detrimental if their levels become too high. High levels of ROS, or oxidative stress (OS), are one of the main causes of toxic mechanisms (Blanco et al., 2020). The easy, green, and energy-saving fabrication of

high-performance electrocatalysts toward detecting trace amounts of H₂O₂ in different media remains challenging for a sustainable future. Moreover, H₂O₂ is a byproduct of enzyme-catalyzed reactions such as glucose oxidase (GOx), lactate oxidase (LOx), urate oxidase (UOx), and cholesterol oxidase (ChoOx) (ShamkhaliChenar and Choi, 2020; Dhara and Mahapatra, 2019). As we all know, human blood glucose concentration is an important indicator to measure human metabolic state and health, especially, hyperglycemia is one of the most typical characteristics of diabetics (Wang et al., 2017). Therefore, close monitoring the blood concentration levels of H₂O₂ and glucose is essential for early diagnosis.

Recently, the vigorous development and commercial success of portable, wearable flexible electronic products have made people's lives more comfortable (Kwak et al., 2012; Boland, 2010). Among them, flexible electronic devices have become a research hotspot due to their broad application prospects in biomedical devices and wearable devices (Long et al., 2020; Wang et al., 2020). In order to accurate detection of

* Corresponding authors.

E-mail addresses: zhiweilu@sicau.edu.cn (Z. Lu), hjdu51@163.com (H. Du), rhb@sicau.edu.cn (H. Rao).

glucose and H_2O_2 level in blood, flexible glucose sensors can easily realize the point of care diagnostic and mobile health by contacting the surface of the skin. Moreover, compared with other optical detection methods, electrochemical sensing has become most common method over the past decades due to its advantages of simple application, high sensitivity and low cost (Ganjali, 2017; Tajik and Beitollahi, 2019; Beitollahi et al., 2019; Mahmoudi-Moghaddam et al., 2019; Ganjali, 2018). Therefore, flexible glucose electrochemical sensors have broad application prospects in portable and wearable health monitoring equipment.

To make electronic devices and sensors flexible, it is usually necessary to choose a suitable flexible material as the substrate, such as polyurethane (Wang et al., 2019), polydimethylsiloxane (PDMS) (Yang et al., 2020), polyetherimide (PEI) (Cheng et al., 2017), polyimide (PI) (Lu et al., 2019a), and so on. However, due to the relatively low electrical conductivity of these materials, these materials must be combined with conductive matrix, e.g. graphene (Dhara and Mahapatra, 2017), carbon nanotubes (Kaviyarasu et al., 2019), metal nanoparticles (M NPs) (Huang et al., 2017) and metal oxide (Liu et al., 2013) to form a novel composite, which can improve the performance of the sensor (Dhara and Mahapatra, 2017; Chaichi and Ehsani, 2016). As a flexible substrate, PI films have been widely applied in flexible instruments on account of its excellent flexibility, high tensile strength, thermal stability and excellent chemical durability (Kurra et al., 2019; Liu et al., 2020). For instance, Zhan et al. (Zhang et al., 2020) reported a flexible non-enzyme glucose sensing (Cu NPs-LIG) ground on laser-induced graphene (LIG) decorated with Cu NPs. Surprisingly, patterned porous graphene can be formed by CO_2 infrared laser irradiation PI film that term LIG (Lin et al., 2014), and the LIG exhibited highly conductive. In addition, LIG as non-hazardous and eco-friendly materials for mass production does not require additional reagents and conditions, and is a green synthesis method compared with traditional methods for graphene synthesis in environment protection (Lin et al., 2014).

Thanks to distinct physicochemical properties, e.g. excellent flexibility, good electrical conductivity, and large specific surface areas, graphene serving as a promising support material (Xu et al., 2014), which has appealed great attentions in the electrochemical sensing fields (C.O. C. and N.S. T., 2010; Hao et al., 2018). In addition, they can act as a good electron carrier and conductive medium to combine with different metal nanoparticles, which accelerate electron transport and promote mass transfer kinetics at the surface of the electrode (Shi et al., 2017), thus improving the catalytic activity of nanoparticles. This strategy not only prevents the restacking of graphenes but also ameliorates the distribution of graphenes (Yoon et al., 2020). For example,

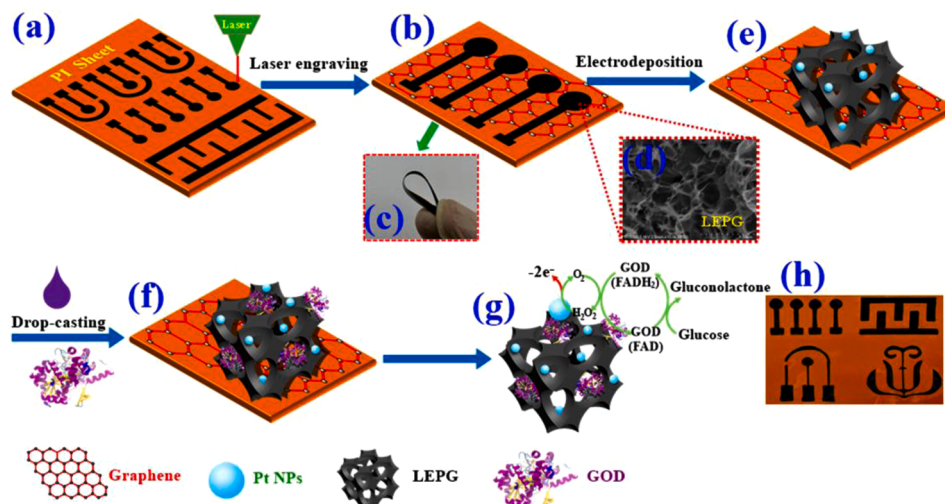
Haxhiaj et al. (2019) reported Pt NPs *in situ* supported on reduced-graphene oxide (rGO) via one-step laser ablation process, which could simultaneously control particle size and mass load. Moreover, in immobilized enzymes catalysts field, graphene-based materials not have great potential, but also can significantly improve the electrochemical behavior of various enzymes, such as glucose oxidase (Zhang et al., 2019), alpha-amylase (Teixeira et al., 2016), horseradish peroxidase (Ye et al., 2019), and catalase (Cao et al., 2020). Therefore, graphene also can be used as flexible electrode material for biosensors. Compared with non-enzymatic sensors, enzymatic sensors work in whole blood (no need to make serum), do not require a dilution step (with the implied risk of infection), and work at pH 6–8 without the need for adding an etching solution such as NaOH. Inspired by this, we believe that the flexible carbon electrode can be prepared by laser scribing and metal-doping of PI films, thus a flexible conductive matrix with micro-patterned can be obtained.

In this work, a flexible, array, micro-patterned, and miniaturized electrode were fabricated by directing laser engraving PI film to formation laser engraving porous graphene (LEPG) at room temperature (Scheme 1 h). After further modification with Pt NPs on activation LEPG (Pt-LEPG) by electrochemical deposition construct H_2O_2 sensor. Subsequently, the flexible and excellent sensitivity for glucose detection amperometric biosensor has been constructed by modification glucose oxidase (GOD) on Pt-LEPG surface (defined as GOD/Pt-LEPG). Hence, the determination of these biomolecules is obtained with high sensitivity of $575.75 \mu\text{A mM}^{-1} \text{cm}^{-2}$ (H_2O_2) for Pt-LEPG, and $241.82 \mu\text{A mM}^{-1} \text{cm}^{-2}$ (glucose) for GOD/Pt-LEPG, respectively, over a wide range of concentration. To our best knowledge, GOD/Pt-LEPG served as sensing material for assay of glucose hasn't been reported. This method is more efficient and simple, proving a new scheme for manufacturing flexible glucose sensor. What's more, the flexible PI substrate will find great potential for applications in wearable or implantable biosensors.

2. Experimental section

2.1. Materials and chemicals

All chemicals are of analytically pure and used without further treatment. Glucose, H_2O_2 (30 %), hexachloroplatinic acid ($\text{H}_2\text{PtCl}_6 \cdot 6\text{H}_2\text{O}$), glucose oxidase (GOD, 113 U mg^{-1}), KH_2PO_4 , Na_2HPO_4 , potassium ferrocyanide ($\text{K}_4\text{Fe}(\text{CN})_6$) and potassium ferricyanide ($\text{K}_3[\text{Fe}(\text{CN})_6]$ were obtained from Aladdin (Shanghai, China, <https://www.aladdin-e.com>). Polyimide (PI) films (thickness: 125 μm) were obtained from Changzhou Jinlong Insulation Materials Co., Ltd



Scheme 1. Fabrication process and sensing principle of a novel enzymatic flexible sensor based on H_2O_2 and glucose oxidation of GOD/Pt-LEPG.

(Changzhou, China, <http://jinlong.tape168.com>). Phosphate buffer solutions (PBS) were prepared from KH_2PO_4 and Na_2HPO_4 . Ultrapure (UP) water ($18.25 \text{ M}\Omega \text{ cm}$) were utilized throughout.

2.2. Fabrication of LEPG

Commercially Kapton PI films were used as flexible substrates. It was first clean with anhydrous alcohol and UP-water, respectively, and then dried naturally. Subsequently, paste one side of PI film on the glass plate, and the conventional three electrodes were made by JL-3020 touch the high-end laser engraving machine with 50 W of power, 0.05 mm of step size, and $100 \text{ mm} \cdot \text{s}^{-1}$ of speed for engraving under environmental air conditions. The working electrode is designed with a 3 mm diameter. Afterward, Ag/AgCl paste was cast onto a nearby graphene as reference electrode (RE) and a Pt filament as counter electrode (CE). These flexible micro-patterned electrodes are shown in Scheme 1(c). Here, laser engraving graphene array working electrode (WE) is utilized to improve the sensor's stability and flexibility.

2.3. Fabrication of Pt-LEPG and GOD/Pt-LEPG

The synthesis of Pt NPs modification LEPG was performed via the in-situ electrochemical deposition method. Prior to modification, to achieve the best electrochemical capability, the LEPG sheet was activation in PBS solution ($\text{pH} = 7.0$) by CV from 0.8 V to 1.3 V for 25 cycles at $100 \text{ mV} \cdot \text{s}^{-1}$ scan rate. Subsequently, activation LEPG was immersed in 2 mM H_2PtCl_6 solution by CV range 0–0.5 V at $50 \text{ mV} \cdot \text{s}^{-1}$ scan rate to obtained Pt-LEPG electrode. The obtained Pt-LEPG was rinsed with UP-water, and dried naturally. Then, 5 μL GOD diluent (20 mg mL^{-1} in PBS) was dropped at WE of Pt-LEPG until to dry completely. Lastly, the WE's surface was coated 0.5 μL Nafion (0.25 % in ethanol) to obtained GOD/Pt-LEPG for preventing the loss of GOD. Finally, the GOD/Pt-LEPG was stocked in pH 7.0 PBS at 4 °C.

2.4. Characterization and measurement

All fabrication materials were investigated by energy-dispersive X-ray spectroscopy (EDS) mapping, transmission electron microscopy (TEM, JEOL, JEM 2100 F), field-emission scanning electron microscopy (SEM, JEOL JSM 7500 F), X-ray photoelectron spectroscopy (XPS, Thermo Fisher Scientific, USA), X-ray diffraction (XRD, D8 Advance, German), X-ray photoelectron spectroscopy (XPS, ESCALAB 250Xi spectrometer), and Raman spectroscopy (Jobin Yvon LabRAM Aramis spectroscopy), respectively. The LEPG and Pt-LEPG samples for XRD analysis experiments were powder scratched from LEPG and Pt-LEPG films, respectively. The other characterizations, such as Raman spectra, XPS, and SEM were conducted directly on LEPG films. An IGS1230 electrochemical workstation (Guangzhou, China, <http://www.ingsens.com>) was utilized for electrochemical tests, e.g. amperometric curve (i-t), cyclic voltammetry (CV) and AC impedance, respectively.

2.5. Sample treatment

Human serums were supplied from the school hospital. Generally, the serum sample (5.0 mL) was mixed with 5.0 mL PBS ($\text{pH} 7.0$, 0.1 M) and analyzed under optimized i-t conditions. All studies were executed complying with relevant laws and guidelines.

3. Results and discussion

3.1. Sensor design

The fabrication process and working principle of flexible bifunctional H_2O_2 and glucose sensors based on GOD/Pt-LEPG are illustrated in Scheme 1. First of all, a laser beam was used to irradiate the directly flexible PI sheet in the ambient air. Due to the photothermal effect, the

PI film was rapidly be carbonized from orange to black at a temperature higher than 2000 °C (Lu et al., 2019a), which is accompanied by the generation of graphene and embedded in the PI sheet (Scheme 1a-c). The resulting product is named as 3D LEPG with porous structures (Scheme 1d). After that, Pt NPs were selectivity anchored on the electrode area by electrochemical cyclic voltammetry deposition to formation Pt-LEPG (Scheme 1e). Subsequently, the Pt-LEPG was been immobilized of glucose oxidase (GOD) to the fabrication GOD/Pt-LEPG electrode (Scheme 1f). As display in Scheme 1h, different micro and miniaturized patterned electrodes were formatted by directing laser engraving process, such as array electrode, co-planar three-electrode, comb-like and flower-like patterned. Finally, newly-designed GOD-/Pt-LEPG array electrode realizes the sensing of H_2O_2 and glucose. Pt NPs can directly oxidize H_2O_2 to oxygen and produce two electrons, resulting in current response, thus achieving quantitative analysis and detection H_2O_2 (Yoon et al., 2020). The glucose molecules are oxidized by GOD (flavin adenine dinucleotide, FAD) to gluconolactone, the active center of enzyme (FAD) is reduced to FADH_2 at the same time (Scheme 1e). However, FADH_2 can reduce oxygen to H_2O_2 and itself is oxidized to FAD. Combined with Pt NPs catalytic oxidation of H_2O_2 and voltammetric response, a highly sensitive electrochemical glucose sensing was established on GOD/Pt-LEPG.

3.2. Characterization of the modified materials

The morphological characterization of LEPG, Pt-LEPG, and GOD/Pt-LEPG was observed by TEM and SEM. From Fig. 1a, obvious groove structures were induced by laser engraving directly on PI sheets. With on the enlarged image of LEPG (Fig. 1b), the connected porous structures and thin layers graphene can be clearly seen, which is mainly caused by the carbonization of PI sheet at high temperature (Singh et al., 2017). Obviously, these hierarchical porous structures of LEPG can enhance the accessible surface areas, accelerate electron transfer, and supply abundant active sites. The FE-SEM images of Pt-LEPG exhibited Pt NPs (ca. 180 nm in diameter) were uniformly anchored on graphene sheet surface in Fig. 1(c-d). Besides, as the number of deposition segments of CV implementation was increased, the state of morphology the as-produced Pt NPs look different. As shown in Fig. 1S, uniform dispersion of Pt NPs was also observed by the number of deposition segments is 10 segments (5 cycles). For Fig. 1(e-f), it was observed that the surface of Pt-LEPG was uniformly coated with glucose oxidase (GOD). The TEM image in Fig. 1g indicates uniform dispersion of Pt NPs and a very thin graphene sheet on LEPG. A closer observation in high-resolution Fig. 1h exhibits the uniform Pt NPs ca. 5 nm in diameter are encapsulated by graphite layers. The presence of Pt NPs and graphitic carbon structures were clearly demonstrated by High-resolution TEM (HRTEM). The d-spacing of 0.277 nm and 0.335 nm correspond to these lattice fringes of Pt (111) and C (002) (Nayak et al., 2016), respectively. Besides, the distributions of different species were further identified by the elementals mappings, revealing the mainly composed of C, N, O and evenly decorated Pt NPs on LEPG (Fig. 1i).

The LEPG and Pt-LEPG were characterized by XRD in Fig. 2A. It presents a convex peak at $2\theta = 24.68^\circ$ (002) matching to the graphitic crystal phase with the interlamellar spacing of 0.36 nm, and a weak peak at nearby 43.03° (101) belong to an in-plane structure (Lu et al., 2019a). The presence of (002) plane and (101) plane may be attributed to turbostratic and graphitized carbon, respectively, which demonstrated that both LEPG and Pt-LEPG with a high level of graphitization (Lu et al., 2019b). Generally speaking, XRD characterization results confirm that the prepared LEPG and Pt-LEPG are exactly graphene. Besides, the XRD images of Pt-LEPG also demonstrated that there were another five peaks matching the standard XRD. Specifically, upon incorporating Pd NPs onto the LEPG substrate, five additional peaks at $2\theta = 39.76^\circ$, 46.24° , 67.45° , 81.29° , and 85.71° , respectively, corresponding to the (111), (200), (330), (311), and (222) index planes of the face-centered cubic (fcc) crystalline Pt metal cube structures (JCPDS No. 04-0802) were

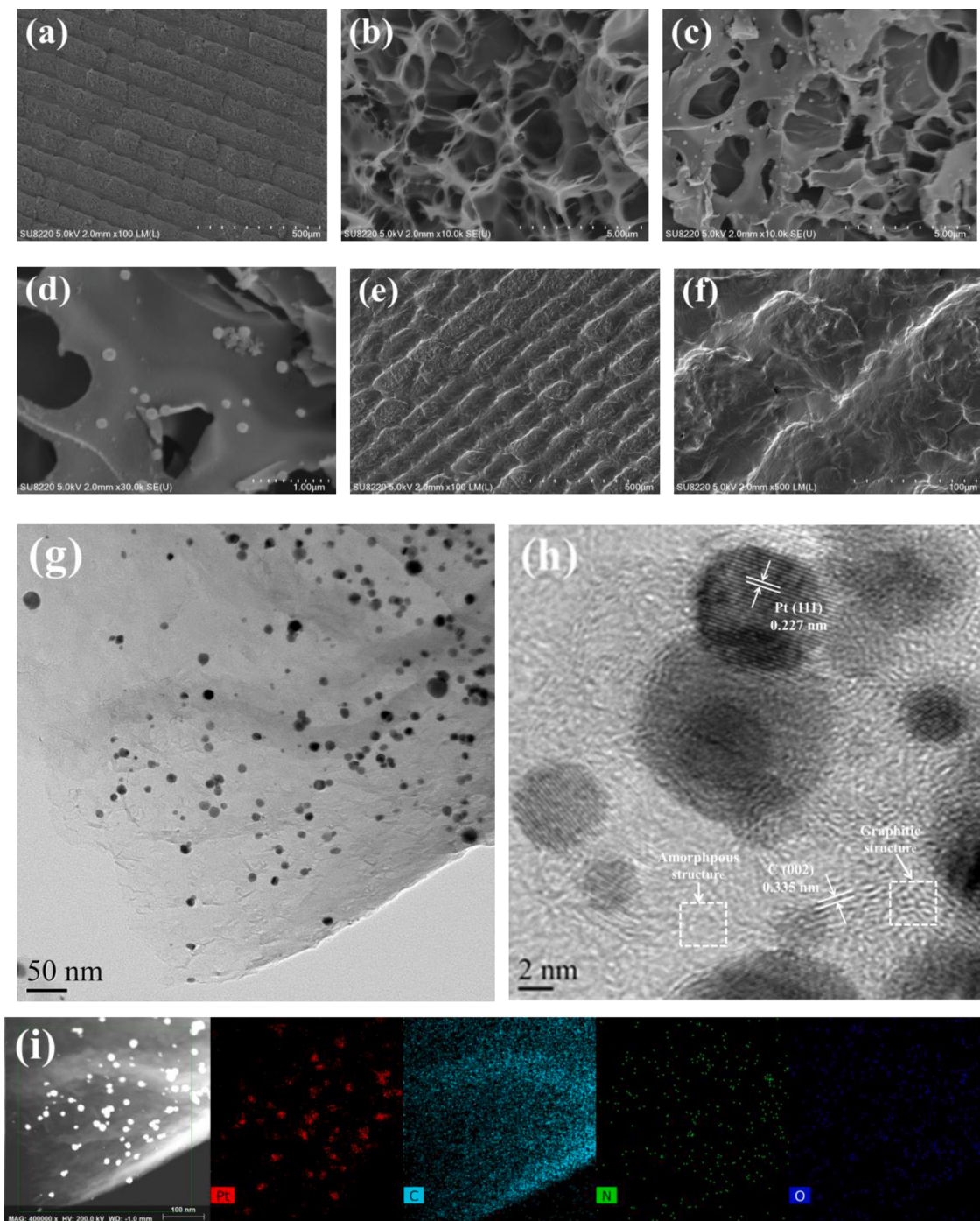


Fig. 1. FE-SEM images of LEPG (a-b), Pt-LEPG (c-d), and GOD/Pt-LEPG (e-f), respectively. (g) TEM image and (h) HRTEM image of Pt-LEPG; (i) STEM and elemental mappings (Pt, C, N, O) of Pt-LEPG.

observed (Nayak et al., 2016). In addition, according to the Scherrer' equation by analyzing the XRD diffraction peaks, the average particle size of Pt NPs was estimated from the Pt (111) diffraction peak to be ca. 5.8 nm, which is consistent with the average diameter observed in the TEM. These results suggested that Pt nanoparticles are indeed loaded on the LEPG to the formation of Pt-LEPG.

The Raman spectra of LEPG and Pt-LEPG show three characteristic bands: D-band at ca. 1350 cm^{-1} , G-band at ca. 1588 cm^{-1} , and 2D-band at ca. 2697 cm^{-1} (Fig. 2B). D peak implies the structure defects nature, and G peak suggests the E_{2g} vibration nature of graphitic carbon (Lin et al., 2014). The crystalline quality of LEPG and Pt-LEPG was quantitatively evaluated via the intensity ratio (I_D/I_G) between d-band and

G-band. The typical I_D/I_G ratios are 0.97 and 1.12, respectively. A high ratio of Pt-LEPG indicated that a high degree crystal defect was formed, possibly ascribed to anchor Pt NPs introduces more defects (Nayak et al., 2016). However, the rise of the 2D peak of LEPG and Pt-LEPG (Fig. 2B) further confirmed the existence of 2D graphene nanosheet structure, which was consistent with SEM and TEM analysis results.

In addition, the surface chemical states and chemical compositions of Pt-LEPG were investigated by XPS. As shown in the full spectra in Fig. 2C, Pt-LEPG consists of C, N, O, and Pt elements compared to the LEPG consisting of C, Pt, N, and O elements. Compared with LEPG, the existence of Pt peak in Pt-LEPG, despite the lower content of Pt (0.73 %), successful electrodeposition of Pt NPs onto LEPG was confirmed again.

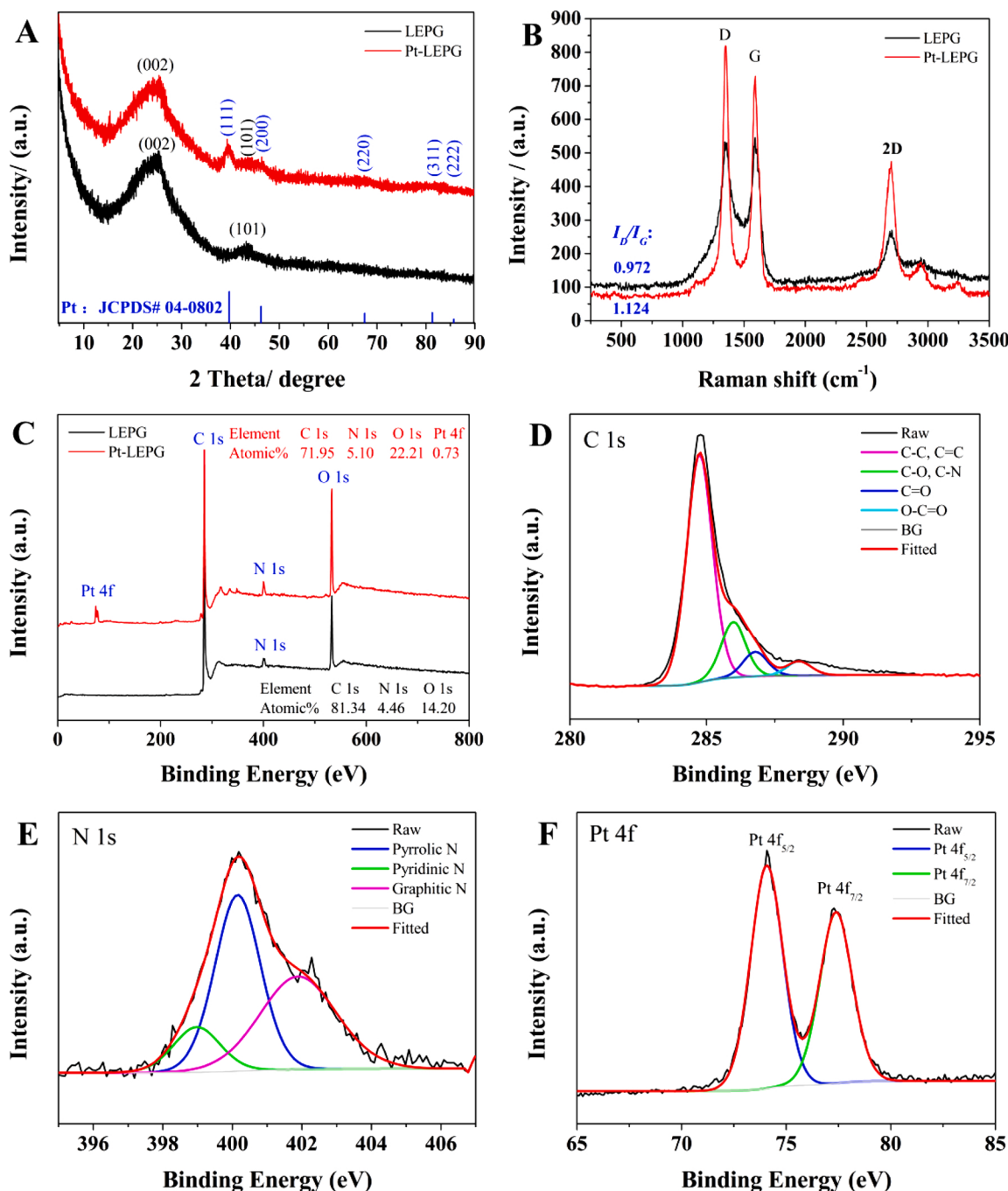


Fig. 2. Characterization of LEPG and Pt-LEPG. (A) XRD pattern and (B) Raman spectrum. (C) XPS survey, (D) C 1s, (E) N 1s, and (F) Pt 4f spectra of Pt-LEPG, respectively.

The C 1s peaks can be assigned to the C-C & C=C (284.6 eV), C-O & C-N (285.9 eV), C=O (286.8 eV), and O-C=O (288.3 eV), respectively (Fig. 2D) (Lu et al., 2018). Furthermore, the N 1s high-resolution spectrum revealed the existence of three varieties of nitrogen, namely pyridinic N (398.9 eV), pyrrolic N (400.2 eV), and graphitic N (401.2 eV), respectively (Fig. 2E). Noteworthy that pyrrolic N and pyridine N dominate in Pt-LEPG, suggesting that these N atoms have greater thermodynamic stability at the edge of the graphene lattice, which is consistent with theoretical predictions (Liu et al., 2020). In addition, according to relevant literature reported, graphitic N, pyridine N, and pyrrolic N could effectively enhance electro-catalytic properties and electronic conductivity of N-doped carbon-based material (Hao et al., 2018; Xu et al., 2017). Thus, Pt-LEPG composites were endowed with

higher electrocatalytic activity. As shown in Fig. 2F, the peaks of Pt 4f can be divided into two main components: Pt 4f_{5/2} (74.0 eV) and Pt 4f_{7/2} (77.4 eV). However, the XPS characteristics of Pt 4f doublet are attributed to the generation of zero-valent Pt NPs (Pt(0)) by electrochemical deposition (Chen et al., 2018). Therefore, the above results indicate that graphitized graphene can be obtained by laser engraving directly on the PI membrane, which is an attractive process.

3.3. Electrochemical characterization measurements

Electrochemical performances of the modified electrode were identified by CV and EIS techniques. The CV curves of the electrodes illustrated the characterization of the manufacturing process (Fig. 3A). All

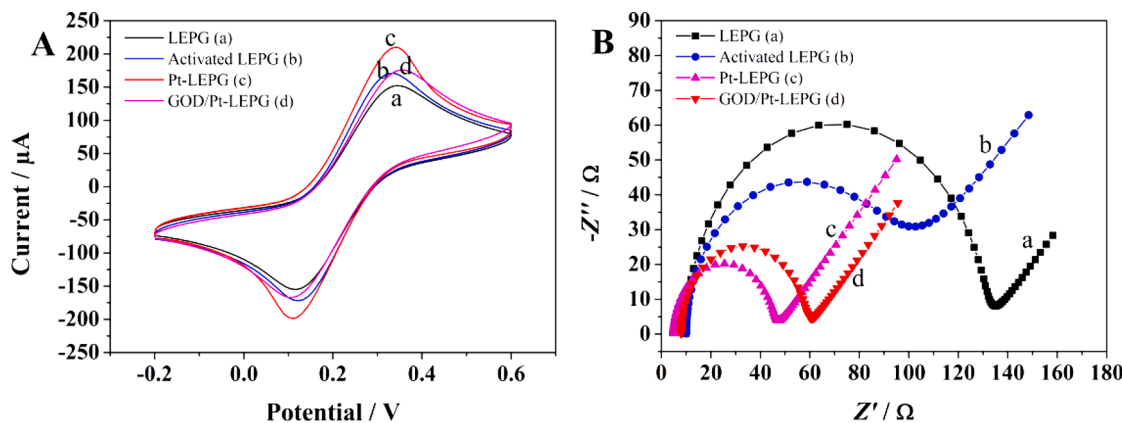


Fig. 3. (A) CV curves and (B) EIS spectrum of LEPG (a), activated LEPG (b), Pt-LEPG (c), and GOD/Pt-LEPG (d) were obtained in $[Fe(CN)_6]^{3-/4-}$ (5 mM) containing 0.1 M KCl, respectively.

the modified electrodes exhibited a pair of well-distinct redox characteristic peaks. Based on the good conductivity of graphene could facilitate the electrode transfer, while the hierarchical porous network structures of LEPG is helpful for the $[Fe(CN)_6]^{3-/4-}$ redox probe diffuse to the LEPG surface (*curve a*). Interestingly, after electrochemical activation in PBS (0.1 M, pH 7.0), the peak current of activation LEPG is significantly increased (*curve b*). This was mainly ascribed to the large amount of organic adhesive removed after activation, and micron-sized graphite particles clearly exposed to the electrode surface after electrochemical pretreatment. This is in agreement with our previous studies showing that the activated LEPG surface-exposed more active sites (Lu et al., 2019a). Thus, these observations reveal that electrochemical activation pretreatment processes considerably affect the surface cyclic voltammetry properties, and the activated electrode behaves like a random array microelectrode with increased heterogeneous electron transfer rates (Su et al., 2011). After LEPG decorated with Pt NPs (*curve c*), the redox peak currents increased significantly could be ascribed the good electrical conductivity of metal Pt NPs, which permitted increasing the active areas of Pt-LEPG electrode. As expected, the redox peak currents decreased after introduction of GOD on Pt-LEPG due to GOD membrane impedes the electron transfer between $[Fe(CN)_6]^{3-/4-}$ and the electrode surface (*curve d*). These results indicate that GOD and Pt NPs have successfully incorporated graphene.

The surface characteristics of the electrode during each step of modification were further investigated by EIS (Fig. 3B). The typical Nyquist spectrum composed of a lower frequency region for a linear part and a higher frequency range for semicircle part, corresponding to the diffusion process and electron transfer, respectively (Lu et al., 2017). LEPG exhibits the largest electron transfer resistance (R_{CT}) of 130 Ω

(*curve a*). After electrochemical activation (*curve b*), the R_{CT} value of activation LEPG is significantly reduced to 110 Ω due to the high surface activity. However, Pt-LEPG shows the smallest R_{CT} of 45 Ω (*curve c*), which may be contribution by the synergistic effect between high-mass transfer rate of Pt NPs, and high surface activity of LEPG. This suggests that when Pt NPs anchored on LEPG surface, it easily helps to enhance the conduction pathway. Following the incorporation of GOD, the R_{CT} value of GOD/Pt-LEPG (55 Ω) significantly increased (*curve d*) compared to Pt-LEPG. This phenomenon is mainly due to the enzyme molecules on the electrode surface blocking the redox probes to reach the electrode surface (Cheng et al., 2015). These EIS results concur with CV results, and these also proved the successful formation of GOD/Pt-LEPG. Besides, the effective active areas of modified electrodes were calculated as 0.0041 cm^2 of LEPG, 0.0047 cm^2 of Pt-LEPG and 0.0059 cm^2 of GOD/Pt-LEPG, respectively (Fig. S2). In contrast to the smaller effective area of LEPG, the surface area of Pt-LEPG is obviously increased, which could be attributed to the synergistic effect between the good conductivity of Pt NPs and large surface area of LEPG.

3.4. Sensing performance for H_2O_2 detection

The electro-catalytic performances of H_2O_2 by various modified electrodes were investigated by CVs. For comparison, LEPG and Pt-LEPG were tested under the same conditions with and without 5 mM H_2O_2 , respectively. Neither LEPG nor Pt-LEPG observed peaks in the PBS electrolyte of pH 7.0, as displayed in Fig. 4 (solid lines). However, in the presence of 5 mM H_2O_2 , both LEPG and Pt-LEPG exhibit a pair of redox peak (dotted lines). For LEPG, the anodic onset potential is approximately +0.400 V, while cathode onset potential is about -0.218 V.

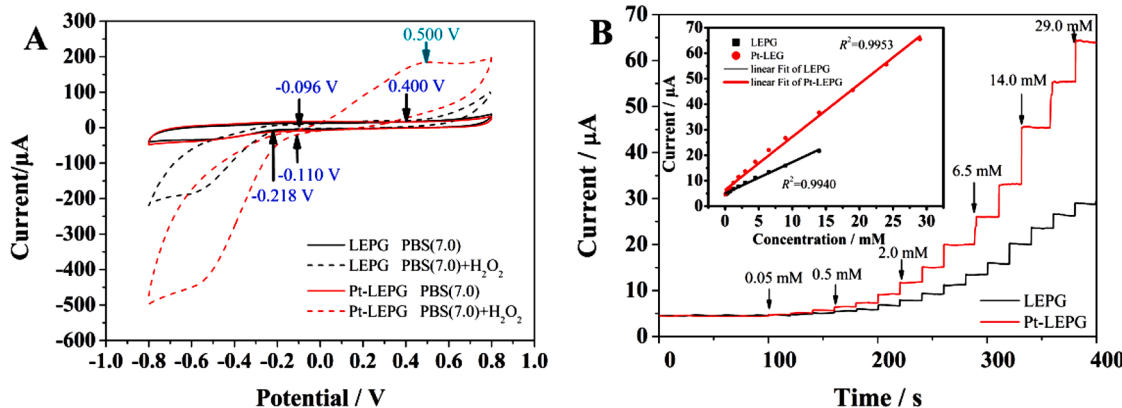


Fig. 4. (A) CV curves of LEPG and Pt-LEPG in PBS (pH 7.0) with or without 5 mM H_2O_2 . (B) i-t curves at +0.5 V for successive addition H_2O_2 . (Insert: corresponding calibration curves).

Table 1

Analytical performances of various modified electrodes for glucose detection.

Electrode	Method	Applied potential (V)	Equation	Linear range (mM)	Sensitivity ($\mu\text{A mM}^{-1} \text{cm}^{-2}$)	Detect limit (μM)	R^2	Ref
GOD/Pt-LEPG	i-t	+0.6	i = 1.336C + 0.311	0.01–3.05	226.44	0.10	0.9905	
			i = 1.336C + 0.311	3.05–31.5			0.9623	
Pt-LEPG	i-t	+0.6	i = 0.538C + 0.320	0.005–2.16	114.47	0.05	0.9905	This work
			i = 0.029C + 1.261	2.16–12.41			0.9919	
LEPG	i-t	+0.6	i = 0.051C + 0.040	0.225–4.725	12.44	2.7	0.9824	
			i = 0.025C + 0.251	4.725–18.225			0.9901	
GN/FAD/apo-GOx/Nf/SPCE	CV	+0.475	i = 0.000625C - 0.01015	50–250 mg L^{-1}	—	20 mg L^{-1}	0.99253	(Mehmeti et al., 2017)
			i = 0.000375C + 0.058424	250–2000 mg L^{-1}			0.99927	
CS/Pd@Pt NC/GOx	i-t	-0.650	—	1–6	6.82	0.2	—	(Krishnan et al., 2017)
GOD/Pt/FGS/Cs/GCE	i-t	+0.4	—	0.2–5	—	0.6	—	(Wu et al., 2009)
Au-NiO/Ni(OH) ₂ -GOx	CV	-0.6	i = -0.0392C - 0.475	6–30	1.95	1.54 mM	0.9991	(Njoko et al., 2020)
PtNWA/AuNPs/GOD	CV	+0.3	—	15–2500	184	15	0.997	(Li et al., 2017)
GOD/Pt-MWCNTs/CSF	CV	+0.65	—	0–5	288.86	50	0.991	(Chen et al., 2018)

Compared with LEPG, the anodic and cathode onset potentials are -0.096 V and -0.110 V, which is negatively shifted of 409 mV and positive shifted of 108 mV, respectively. These results indicate the catalysis of LEPG and Pt-LEPG on H_2O_2 can choose either positive potential or negative potential as the working potential (Lu et al., 2019c). Meanwhile, for Pt-LEPG, the oxidation peak current is +184.12 μA at +0.5 V while reduction peak current is -400.28 μA at -0.5 V, which is 7.37 times for anodic current response than of LEPG (24.98 μA) and 2.64 times for cathode current response than of LEPG (-151.30 μA), respectively. Considering the influence of high potential water oxidation, therefore +0.5 V was selected as the best potential for further experiments to assay sensor performance. The excellent electrocatalytic performance of Pt-LEPG is mainly due to its high conductivity of Pt NPs, abundant active sites of porous graphene network, and nitrogen doping properties.

The typical current-times (i-t) response curves of the LEPG and Pt-LEPG with continuous addition H_2O_2 at different concentrations in PBS are shown in Fig. 4B. Observed that i-t response curves were obviously in the shape of the stair step with the increase of H_2O_2 concentration, and the response of steady-state current is achieved within 0.1 s, indicating that both LEPG and Pt-LEPG possessed excellent electrochemical catalytic performance. For LEPG, a fitted calibration curve between current response and H_2O_2 concentration is $I(\mu\text{A}) = 1.226 C_{\text{H}_2\text{O}_2} (\text{mM}) + 5.062$ ($R^2 = 0.9940$) at 50 μM –14 mM, with a detection limit (LOD) of 3.8 μM ($S/\text{N} = 3$). However, the response calibration equation of Pt-LEPG is $I(\mu\text{A}) = 2.076 C_{\text{H}_2\text{O}_2} (\text{mM}) + 6.463$ ($R^2 = 0.9953$) at 10 μM –29 mM, together with a LOD is 0.65 μM ($S/\text{N} = 3$). Besides, the response sensitivity of Pt-LEPG is 575.75 $\mu\text{A mM}^{-1} \text{cm}^{-2}$, which is 1.9 times of LEPG.

3.5. Optimization of experimental parameters

The following parameters were optimized: (a) The number of deposition segments; (b) pH value of electrolyte solution; (c) applied potential. Respective text and Figures on optimizations are given in the Electronic Supporting Material. In short, the following experimental conditions were found to give the best results: (a) Best deposition segments: 6; (b) pH 7.0 of 0.1 M PBS; and (c) optimum applied potential: +0.5 V.

3.6. Glucose sensing performance of the biosensor

Fig. 5 shows the relationships between current responses and the concentrations of successive injection glucose at +0.5 V. The typical i-t curves of the modified electrode for glucose are shown in Fig. 5A, Fig. 5C, and E, respectively. With each glucose injection, response

currents increased promptly and achieved the steady-state currents within 7 s for LEPG, 5 s for Pt-LEPG, and 0.1 s for GOD/Pt-LEPG, respectively. This reason may be due to the fact that glucose molecules were rapidly absorbed and activated on the surface of GOD/Pt-LEPG. The corresponding calibration curves for peak current vs. glucose concentration are shown in Fig. 5B, D, and F, respectively. Results indicated that all modified electrode's calibration plots are linear with two sections (Table 1). For GOD/Pt-LEPG sensor, such a broad area of quantification (0.01–31.5 mM) would facilitate the utility of analysis. Moreover, the sensitivity was found to approach 241.82 $\mu\text{A mM}^{-1} \text{cm}^{-2}$, and the LOD was calculated to be 0.10 μM ($S/\text{N} = 3$), which was advantageous to that on LEPG and Pt-LEPG. Besides, it was found that the GOD/Pt-LEPG exhibits excellent performance as compared with reported enzyme glucose sensors in physiological pH of 7.4 according to Table 1. This further verified the outstanding analytical performance of the prepared sensor.

3.7. Selectivity, reproducibility and stability

To evaluate the specificity of the sensor, we challenged the potential impact of some compounds with redox ability on the system, i.e. glucose (2.5 mM), uric acid (UA, 1.0 mM), dopamine (DA, 1.0 mM), glucose (1.0 mM), ascorbic acid (AA, 1.0 mM), sucrose (1.0 mM), fructose (1.0 mM), maltose (1.0 mM), L-cysteine (1.0 mM), glutathione (1.0 mM), acetaminophen (1.0 mM), glucose (1.0 mM) and glucose (1.0 mM). As expected, the presence of potentially interfering substances did not affect obvious current changes of the GOD/Pt-LEPG sensor (Fig. 6A). These results show that GOD/Pt-LEPG sensor has a good selectivity for the determination of glucose. To evaluate the reproducibility of GOD/Pt-LEPG, the same modified electrode was compared in five electrolytes (pH 7.0, PBS) with the same glucose concentration (1 mM), respectively. Obviously, the current response has no significant change, and the relative standard deviation (RSD) is low of 7.37 % (Fig. 6B), implying that as-prepared sensor has good reproducibility. In addition, the electrode was stocked in PBS (0.1 M, pH 7.0) at 4 °C, and the electrode's long-term sensing stability was evaluated by continuous detecting 0.5 mM glucose every day for two weeks. The decrease in the amperometric response of GOD/Pt-LEPG was not significant with the RSD value of 10.6 % over two weeks (Fig. 6C), indicating acceptable long-term stability to glucose detection.

3.8. Analysis of actual samples

To evaluate the utility of this biosensor, human serum samples (obtained from the university hospital) with known glucose concentrations

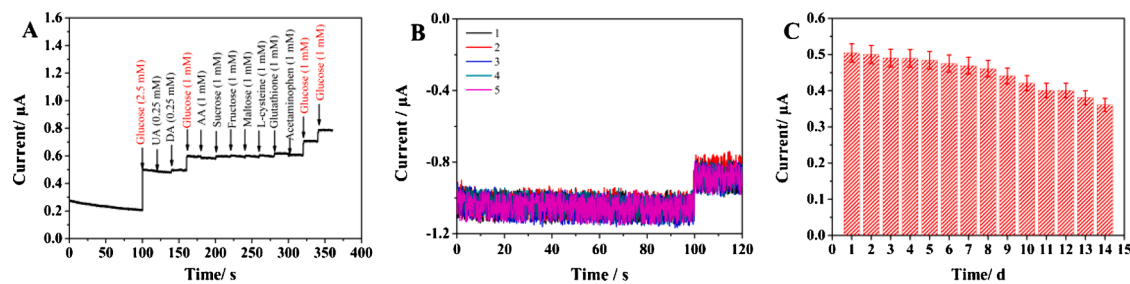


Fig. 6. (A) Interference and (B) reproducibility response of GOD/Pt-LEPG sensor. (C) Long-term stability of the GOD/Pt-LEPG sensor for continuous glucose detection for two weeks. Applied potential: +0.5 V; Electrolyte: pH 7.0 PBS.

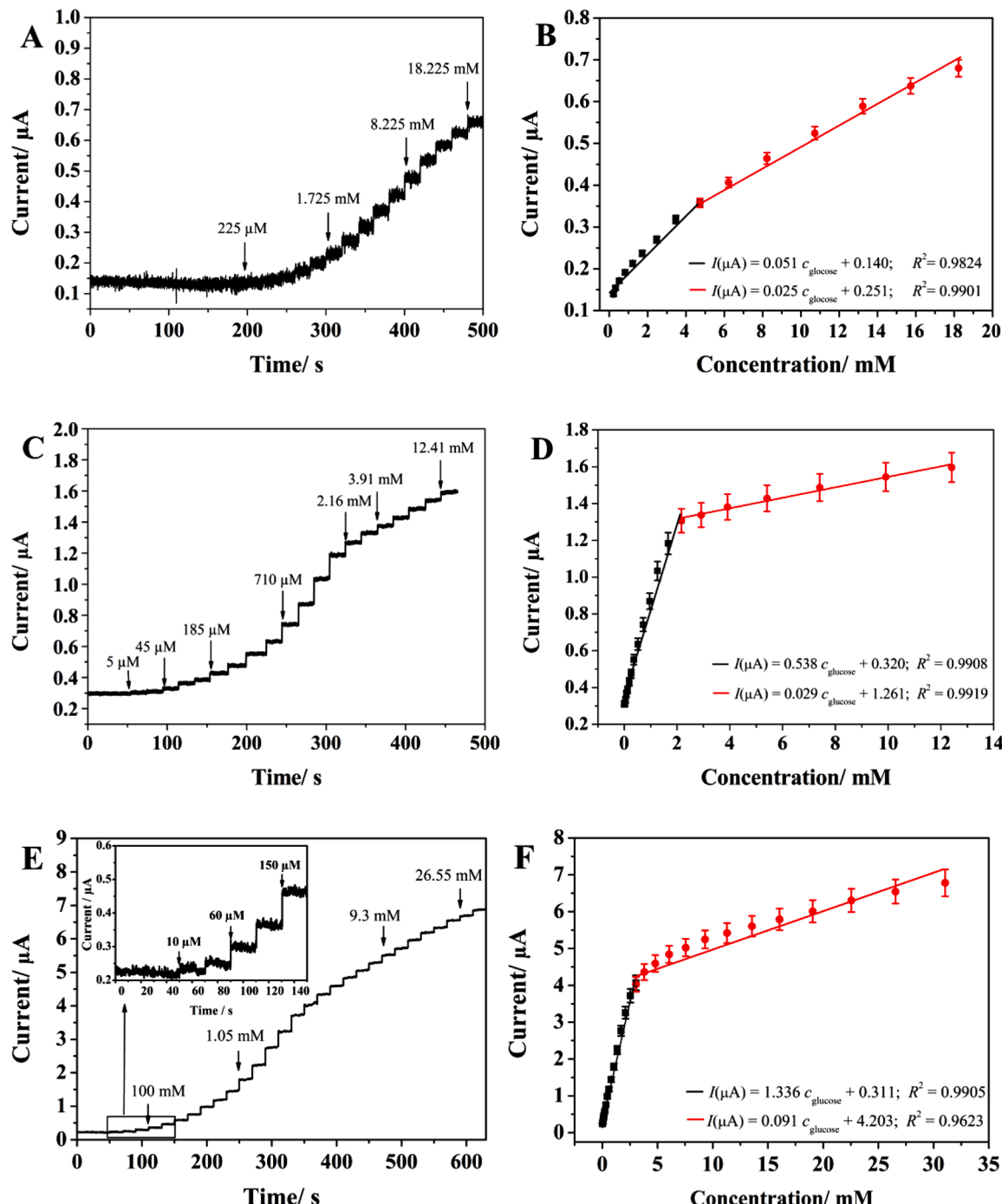


Fig. 5. Amperometric current responses of (A) LEPG, (C) Pt-LEPG, and (E) GOD/Pt-LEPG on the successive addition of glucose into PBS (pH 7.0) at +0.5 V, respectively.; The corresponding calibration curves for the amperometric responses of (B) LEPG, (D) Pt-LEPG, and (F) GOD/Pt-LEPG, respectively.

Table 2

Results obtained for determination of glucose in human serum samples.

samples	Hospital (mM)	This work (mM)	Glucometer (mM)	Addition (mM)	Found (mM)	Recovery (%)
1	7.32	8.13	7.85	5.00	13.06	99.47
2	6.13	6.30	6.04	8.00	14.62	102.24
3	14.95	13.94	14.72	2.00	16.14	101.25

were analyzed. Data from commercial glucose meters and hospital clinical results were compared with these results (Table 2). Obviously, theses amperometric responses of these samples are consistent, indicating that the GOD/Pt-LEPG sensor can be successfully applied for detecting glucose in serum samples. Moreover, the recovery of known spiked glucose to the serum sample was satisfying with values range from 93.24–111.06%.

4. Conclusions

In summary, we describe a simple, novel, and bi-functional amperometric sensor based on GOD/Pt-LEPG for sensitive electrochemical assay of H₂O₂ and glucose at near-neutral pH conditions. The direct laser engraving on flexible PI film is a low cost and high-efficiency methodology to fabricate porous network graphene. This unique structure of LEPG was successfully functionalized with Pt NPs by CV electrodeposition to form Pt-LEPG, exhibiting good conductivity and excellent sensitivity for H₂O₂ sensing. As a result, it can be immobilized glucose oxidase (GOD) and effectively electro-catalyze glucose oxidation in near-neutral pH conditions. Response in the concentration range from 0.01 mM to 31.5 mM is linear, with an ultralow LOD of 0.3 μM (S/N = 3). Due to its excellent performance, LEPG materials have great potentials in the application of flexible energy storage and sensing electronic devices.

CRediT authorship contribution statement

Zhiwei Lu: Writing - original draft, Conceptualization, Investigation, Supervision. **Lan Wu:** Writing - review & editing. **Xianxiang Dai:** Data curation. **Yanying Wang:** Conceptualization. **Mengmeng Sun:** Supervision. **Cailong Zhou:** Resources, Funding acquisition. **Haijun Du:** Resources, Funding acquisition. **Hanbing Rao:** Resources, Funding acquisition, Project administration, Supervision.

Declaration of Competing Interest

The authors declare no conflict of interest.

Acknowledgments

The authors thank the financial support of this work by Two-Way Support Team Programs of Sichuan Agricultural University (Project No. 2021993036), the Natural Science Foundation Project of Chongqing (No. cstc2019jcyj-msxmX0309), and the National Natural Science Foundation of China (Grant No. 21905186, 81860701).

Appendix A. Supplementary data

Supplementary material related to this article can be found, in the online version, at doi:<https://doi.org/10.1016/j.jhazmat.2020.123774>.

References

- Beitollahi, H., Movahedifar, F., Tajik, S., Jahani, S., 2019. A review on the effects of introducing CNTs in the modification process of electrochemical sensors. *Electroanalysis* 31, 1195–1203.
- Blanco, E., Vázquez, L., del Pozo, M., Roy, R., Petit-Domínguez, M.D., Quintana, C., Casero, E., 2020. Evaluation of oxidative stress: nanoparticle-based electrochemical sensors for hydrogen peroxide determination in human semen samples. *Bioelectrochemistry* 135, 107581.
- Boland, J.J., 2010. Within touch of artificial skin. *Nat. Mater.* 9, 790–792.
- C.O. C, N.S. T, 2010. Graphene oxide, highly reduced graphene oxide, and graphene: versatile building blocks for carbon-based materials. *Small* 6, 711–723.
- Cao, J.-T., Fu, X.-L., Liu, F.-R., Ren, S.-W., Liu, Y.-M., 2020. Reduced graphene oxide-gold nanoparticles-catalase-based dual signal amplification strategy in a spatial-resolved ratiometric electrochemiluminescence immunoassay. *Analyst* 145, 91–96.
- Chaichi, M.J., Ehsani, M., 2016. A novel glucose sensor based on immobilization of glucose oxidase on the chitosan-coated Fe₃O₄ nanoparticles and the luminol-H₂O₂-gold nanoparticle chemiluminescence detection system. *Sens. Actuators B Chem.* 223, 713–722.
- Chen, C., Ran, R., Yang, Z., Lv, R., Shen, W., Kang, F., Huang, Z.-H., 2018. An efficient flexible electrochemical glucose sensor based on carbon nanotubes/carbonized silk fabrics decorated with Pt microspheres. *Sens. Actuators B Chem.* 256, 63–70.
- Cheng, Y.-m., Fa, H.-b., Yin, W., Hou, C.-j., Huo, D.-q., Liu, F.-m., Zhang, Y., Chen, G., 2015. A sensitive electrochemical sensor for lead based on gold nanoparticles/nitrogen-doped graphene composites functionalized with l-cysteine-modified electrode. *J. Solid State Electrochem.* 20, 327–335.
- Cheng, Y., Wang, C., Zhong, J., Lin, S., Xiao, Y., Zhong, Q., Jiang, H., Wu, N., Li, W., Chen, S., Wang, B., Zhang, Y., Zhou, J., 2017. Electrospun polyetherimide electret nonwoven for bi-functional smart face mask. *Nano Energy* 34, 562–569.
- Dhara, K., Mahapatra, D.R., 2017. Electrochemical nonenzymatic sensing of glucose using advanced nanomaterials. *Microchim. Acta* 185, 49.
- Dhara, K., Mahapatra, D.R., 2019. Recent advances in electrochemical nonenzymatic hydrogen peroxide sensors based on nanomaterials: a review. *J. Mater. Sci.* 54, 12319–12357.
- Ganjali, M., 2017. Application of Fe3O4@SiO2/MWCNT film on glassy carbon electrode for the sensitive electroanalysis of levodopa. *Int. J. Electrochem. Sci.* 12, 5243–5253.
- Ganjali, M., 2018. Voltammetric determination of dopamine using glassy carbon electrode modified with ZnO/Al₂O₃ nanocomposite. *Int. J. Electrochem. Sci.* 13, 2519–2529.
- Hao, N., Hua, R., Chen, S., Zhang, Y., Zhou, Z., Qian, J., Liu, Q., Wang, K., 2018. Multiple signal-amplification via Ag and TiO₂ decorated 3D nitrogen doped graphene hydrogel for fabricating sensitive label-free photoelectrochemical thrombin aptasensor. *Biosens. Bioelectron.* 101, 14–20.
- Haxhiaj, I., Tigges, S., Firla, D., Zhang, X., Hagemann, U., Kondo, T., Nakamura, J., Marzun, G., Barcikowski, S., 2019. Platinum nanoparticles supported on reduced graphene oxide prepared in situ by a continuous one-step laser process. *Appl. Surf. Sci.* 469, 811–820.
- Huang, B., Wang, Y., Lu, Z., Du, H., Ye, J., 2017. One pot synthesis of palladium-cobalt nanoparticles over carbon nanotubes as a sensitive non-enzymatic sensor for glucose and hydrogen peroxide detection. *Sens. Actuators B Chem.* 252, 1016–1025.
- Kaviyarasu, K., Mola, G.T., Oseni, S.O., Kanimozi, K., Magdalane, C.M., Kennedy, J., Maaza, M., 2019. ZnO doped single wall carbon nanotube as an active medium for gas sensor and solar absorber. *J. Mater. Sci.: Mater. Electron.* 30, 147–158.
- Kim, M., Kim, S.H., Lee, J.-H., Kim, J., 2020. Unravelling lewis acidic and reductive characters of normal and inverse nickel-cobalt thiospinels in directing catalytic H₂O₂ cleavage. *J. Hazard. Mater.* 392, 122347.
- Krishnan, S.K., Prokhorov, E., Bahena, D., Esparza, R., Meyyappan, M., 2017. Chitosan-covered Pd@Pt core–Shell nanocubes for direct Electron transfer in electrochemical enzymatic glucose biosensor. *ACS Omega* 2, 1896–1904.
- Kurra, N., Jiang, Q., Nayak, P., Alshareef, H.N., 2019. Laser-derived graphene: a three-dimensional printed graphene electrode and its emerging applications. *Nano Today* 24, 81–102.
- Kwak, Y.H., Choi, D.S., Kim, Y.N., Kim, H., Yoon, D.H., Ahn, S.-S., Yang, J.-W., Yang, W.S., Seo, S., 2012. Flexible glucose sensor using CVD-grown graphene-based field effect transistor. *Biosens. Bioelectron.* 37, 82–87.
- Li, Z., Gao, F., Gu, Z., 2017. Vertically aligned Pt nanowire array/Au nanoparticle hybrid structure as highly sensitive amperometric biosensors. *Sens. Actuators B Chem.* 243, 1092–1101.
- Lin, J., Peng, Z., Liu, Y., Ruiz-Zepeda, F., Ye, R., Samuel, E.L.G., Yacaman, M.J., Yakobson, B.I., Tour, J.M., 2014. Laser-induced porous graphene films from commercial polymers. *Nat. Commun.* 5, 5714.
- Liu, M., Liu, R., Chen, W., 2013. Graphene wrapped Cu₂O nanocubes: non-enzymatic electrochemical sensors for the detection of glucose and hydrogen peroxide with enhanced stability. *Biosens. Bioelectron.* 45, 206–212.
- Liu, H., Xie, Y., Liu, J., Moon, K.-s., Lu, L., Lin, Z., Yuan, W., Shen, C., Zang, X., Lin, L., Tang, Y., Wong, C.-P., 2020. Laser-induced and KOH-activated 3D graphene: a flexible activated electrode fabricated via direct laser writing for in-plane micro-supercapacitors. *Chem. Eng. J.* 393, 124672.
- Long, Y., Chen, Y., Liu, Y., Chen, G., Guo, W., Kang, X., Pu, X., Hu, W., Wang, Z.L., 2020. A flexible triboelectric nanogenerator based on a super-stretchable and self-healable hydrogel as the electrode. *Nanoscale* 12, 12753–12759.
- Lu, Z., Zhang, J., Dai, W., Lin, X., Ye, J., Ye, J., 2017. A screen-printed carbon electrode modified with a bismuth film and gold nanoparticles for simultaneous stripping voltammetric determination of Zn(II), Pb(II) and Cu(II). *Microchim. Acta* 184, 4731–4740.

- Lu, Z., Dai, W., Lin, X., Liu, B., Zhang, J., Ye, J., Ye, J., 2018. Facile one-step fabrication of a novel 3D honeycomb-like bismuth nanoparticles decorated N-doped carbon nanosheet frameworks: ultrasensitive electrochemical sensing of heavy metal ions. *Electrochim. Acta* 266, 94–102.
- Lu, Z., Lin, X., Zhang, J., Dai, W., Liu, B., Mo, G., Ye, J., Ye, J., 2019a. Ionic liquid/poly-L-cysteine composite deposited on flexible and hierarchical porous laser-engraved graphene electrode for high-performance electrochemical analysis of lead ion. *Electrochim. Acta* 295, 514–523.
- Lu, Z., Liu, B., Dai, W., Ouyang, L., Ye, J., 2019b. Carbon network framework derived iron-nitrogen co-doped carbon nanotubes for enhanced oxygen reduction reaction through metal salt-assisted polymer blowing strategy. *Appl. Surf. Sci.* 463, 767–774.
- Lu, Z., Wu, L., Zhang, J., Dai, W., Mo, G., Ye, J., 2019c. Bifunctional and highly sensitive electrochemical non-enzymatic glucose and hydrogen peroxide biosensor based on NiCo₂O₄ nanoflowers decorated 3D nitrogen doped holey graphene hydrogel. *Mater. Sci. Eng., C* 102, 708–717.
- Mahmoudi-Moghaddam, H., Tajik, S., Beitollahi, H., 2019. Highly sensitive electrochemical sensor based on La³⁺-doped Co₃O₄ nanocubes for determination of Sudan I content in food samples. *Food Chem.* 286, 191–196.
- Mehmeti, E., Stanković, D.M., Chaiyo, S., Zavasnik, J., Žagar, K., Kalcher, K., 2017. Wiring of glucose oxidase with graphene nanoribbons: an electrochemical third generation glucose biosensor. *Microchim. Acta* 184, 1127–1134.
- Nayak, P., Kurra, N., Xia, C., Alshareef, H.N., 2016. Highly efficient laser scribed graphene electrodes for on-chip electrochemical sensing applications. *Adv. Electron. Mater.* 2, 1600185–1600195.
- Njoko, N., Louzada, M., Britton, J., Khene, S., Nyokong, T., Mashazi, P., 2020. Bioelectrocatalysis and surface analysis of gold coated with nickel oxide/hydroxide and glucose oxidase towards detection of glucose. *Colloids Surf. B Biointerfaces* 190, 110981.
- Shamkhalianchar, H., Choi, J.-W., 2020. Review—non-Enzymatic hydrogen peroxide electrochemical sensors based on reduced graphene oxide. *J. Electrochem. Soc.* 167, 037531.
- Shi, L., Li, Y., Rong, X., Wang, Y., Ding, S., 2017. Facile fabrication of a novel 3D graphene framework/Bi nanoparticle film for ultrasensitive electrochemical assays of heavy metal ions. *Anal. Chim. Acta* 968, 21–29.
- Singh, S.P., Li, Y., Be'er, A., Oren, Y., Tour, J.M., Arnusch, C.J., 2017. Laser-induced graphene layers and electrodes prevents microbial fouling and exerts antimicrobial action. *ACS Appl. Mater. Interfaces* 9, 18238–18247.
- Su, W.-Y., Wang, S.-M., Cheng, S.-H., 2011. Electrochemically pretreated screen-printed carbon electrodes for the simultaneous determination of aminophenol isomers. *J. Electroanal. Chem.* 651, 166–172.
- Su, P., Zhou, M., Song, G., Du, X., Lu, X., 2020. Efficient H₂O₂ generation and spontaneous OH conversion for in-situ phenol degradation on nitrogen-doped graphene: pyrolysis temperature regulation and catalyst regeneration mechanism. *J. Hazard. Mater.* 397, 122681.
- Tajik, S., Beitollahi, H., 2019. A sensitive chlorpromazine voltammetric sensor based on graphene oxide modified glassy carbon electrode. *Anal. Bioanal. Chem. Res.* 6, 171–182.
- Teixeira, S.R., Lloyd, C., Yao, S., Andrea Salvatore, G., Whitaker, I.S., Francis, L., Conlan, R.S., Azzopardi, E., 2016. Polyaniline-graphene based α -amylase biosensor with a linear dynamic range in excess of 6 orders of magnitude. *Biosens. Bioelectron.* 85, 395–402.
- Wang, X., Zheng, Y., Yuan, J., Shen, J., Hu, J., Wang, A.-J., Wu, L., Niu, L., 2017. Three-dimensional NiCo Layered Double Hydroxide Nanosheets Array on Carbon Cloth, Facile Preparation and Its Application in Highly Sensitive Enzymeless Glucose Detection. *Electrochim. Acta* 224, 628–635.
- Wang, R., Xu, W., Shen, W., Shi, X., Huang, J., Song, W., 2019. A highly stretchable and transparent silver nanowire/thermoplastic polyurethane film strain sensor for human motion monitoring. *Inorg. Chem. Front.* 6, 3119–3124.
- Wang, J., He, J., Ma, L., Zhang, Y., Shen, L., Xiong, S., Li, K., Qu, M., 2020. Multifunctional conductive cellulose fabric with flexibility, superamphiphobicity and flame-retardancy for all-weather wearable smart electronic textiles and high-temperature warning device. *Chem. Eng. J.* 390, 124508.
- Wu, H., Wang, J., Kang, X., Wang, C., Wang, D., Liu, J., Aksay, I.A., Lin, Y., 2009. Glucose biosensor based on immobilization of glucose oxidase in platinum nanoparticles/graphene/chitosan nanocomposite film. *Talanta* 80, 403–406.
- Xu, H., Lin, Z., Zhong, X., Huang, X., Weiss, N.O., Huang, Y., Duan, X., 2014. Holey graphene frameworks for highly efficient capacitive energy storage. *Nat. Commun.* 5, 4554.
- Xu, H., Yan, B., Zhang, K., Wang, J., Li, S., Wang, C., Du, Y., Yang, P., Jiang, S., Song, S., 2017. N-doped graphene-supported binary PdBi networks for formic acid oxidation. *Appl. Surf. Sci.* 416, 191–199.
- Yang, Z., Li, H., Zhang, L., Lai, X., Zeng, X., 2020. Highly stretchable, transparent and room-temperature self-healable polydimethylsiloxane elastomer for bending sensor. *J. Colloid Interface Sci.* 570, 1–10.
- Ye, Y., Yan, W., Liu, Y., He, S., Cao, X., Xu, X., Zheng, H., Gunasekaran, S., 2019. Electrochemical detection of Salmonella using an invA genosensor on polypyrrole-reduced graphene oxide modified glassy carbon electrode and AuNPs-horseradish peroxidase-streptavidin as nanotag. *Anal. Chim. Acta* 1074, 80–88.
- Yoon, H., Nah, J., Kim, H., Ko, S., Sharifuzzaman, M., Barman, S.C., Xuan, X., Kim, J., Park, J.Y., 2020. A chemically modified laser-induced porous graphene based flexible and ultrasensitive electrochemical biosensor for sweat glucose detection. *Sens. Actuators, B* 311, 127866.
- Zhang, J., Li, J., Yang, F., Zhang, B., Yang, X., 2009. Preparation of Prussian blue@Pt nanoparticles/carbon nanotubes composite material for efficient determination of H₂O₂. *Sens. Actuators, B* 143, 373–380.
- Zhang, D., Chen, X., Ma, W., Yang, T., Li, D., Dai, B., Zhang, Y., 2019. Direct electrochemistry of glucose oxidase based on one step electrodeposition of reduced graphene oxide incorporating polymerized l-lysine and its application in glucose sensing. *Mater. Sci. Eng., C* 104, 109880.
- Zhang, Y., Li, N., Xiang, Y., Wang, D., Zhang, P., Wang, Y., Lu, S., Xu, R., Zhao, J., 2020. A flexible non-enzymatic glucose sensor based on copper nanoparticles anchored on laser-induced graphene. *Carbon* 156, 506–513.